Symmetry Assessment by Finite Expansion: application to forensic fingerprints

Anna Mikaelyan and Josef Bigun

School of Embedded and Intelligent Systems
Halmstad University
Halmstad, Sweden, 30118
anna.mikaelyan@hh.se
josef.bigun@hh.se

Abstract: Common image features have too poor information for identification of forensic images of fingerprints, where only a small area of the finger is imaged and hence a small amount of key points are available. Noise, nonlinear deformation, and unknown rotation are additional issues that complicate identification of forensic fingerprints.

We propose a feature extraction method which describes image information around key points: Symmetry Assessment by Finite Expansion (SAFE). The feature set has built-in quality estimates as well as a rotation invariance property. The theory is developed for continuous space, allowing compensation for features directly in the feature space when images undergo such rotation without actually rotating them. Experiments supporting that use of these features improves identification of forensic fingerprint images of the public NIST SD27 database are presented. Performance of matching orientation information in a neighborhood of core points has an EER of 24% with these features alone, without using minutiae constellations, in contrast to 36% when using minutiae alone. Rank-20 CMC is 58%, which is lower than 67% when using notably more manually collected minutiae information.

1 Introduction

Fingerprint images collected at crime scenes are called fingermarks (in USA, latents). These images have poor image quality, preventing the use of automatic extraction of image information. By contrast, if they exist, the mates of fingermarks, called tenprints, are processed automatically to a large extent since they usually have good image quality. Fingermarks have a small amount of descriptive key points, making matching based on only geometry of key point constellation unreliable, and demanding manual augmentation of the descriptive power by information from the image content around key points.

Matching fingerprint images can generally be divided into two categories. The first is based on matching geometric constellations of key points (minutiae, core, etc.) of the fingerprint images and is called minutiae-based. Such methods (e.g. [CCG05], [CCHW97], [RBPV00], [CFM10], [CCG05], [JY00]) are usually fast and reliable on good quality images, but their performance is reduced when image quality or number of key points de-

crease [FAMSAFOG05]. Ordinary image descriptors such as those mentioned above, are not used because the quality of images is too poor to obtain gradient directions reliably.

The second category of methods is used in the case of small fingerprint areas or poor quality images. Here image information around key points, in addition to location of key points and their directions, is utilized. Examples of this include manual ridge counts between key points or correlation combined with rotation as for example, in [BVG+00].

We use the structure tensor (ST) [Big87] in combination with frequency and scale estimation to obtain the orientation image, Sec. 2.1. We model orientation maps in ring-shaped concentric regions around key points and represent them by a complex feature vector, Sec. 2.2. The feature vector is low dimensional and has built-in quality estimates of each of its dimensions via magnitudes, Sec. 3. These quality measures can be directly incorporated into matching metrics of feature vectors using tight inequalities, inequalities that always reach the equality boundary for ideal inputs. Unlike other methods, the suggested feature vector stems from mathematically tractable continuous coordinate transformations in neighborhoods of key points; we think this is well suited for describing low quality images undergoing continuous nonlinear geometric distortions, for example, rotation, skewing, and stretching simultaneously. Section 4 describes the matching metrics used in experiments, which are then presented in Sec. 5.

2 Feature extraction

We start feature extraction with preprocessing the original image by applying a Linear Symmetry Tensor (LST)[1] [Big87], [BBN04], a complex and fully equivalent version of the ordinary structure tensor, Fig. 1, with the purpose of obtaining a reliable dense orientation map of the fingermark. Standard scale parameters for building the orientation image that work for good quality images fail for fingermarks, however. Therefore, a new way of establishing these parameters has been recently proposed [pam14] and was made available to us. The procedure and LST will be summarized in Sec. 2.1.

After the dense orientation image has been obtained, we project ring-shaped areas around key points (in the orientation image) onto the space of harmonic functions, Sec. 2.2. Since few bases and rings are involved, extracted features become low dimensional, and yet the spatial interrelations of direction information are preserved. Findings allow the design ring-shaped complex filters which are rotation invariant, as detailed in Sec. 2.3.

2.1 Preprocessing and Linear Symmetry Tensor

To cope with noisy image information, the Linear Symmetry Tensor is applied iteratively to original images and in combination with the phase of Gabor filters which are adapted to orientation information extracted by LST. LST is used here for modelling and extracting

[1] The term "linear" refers to parallel line structures the tensor is designed to detect.

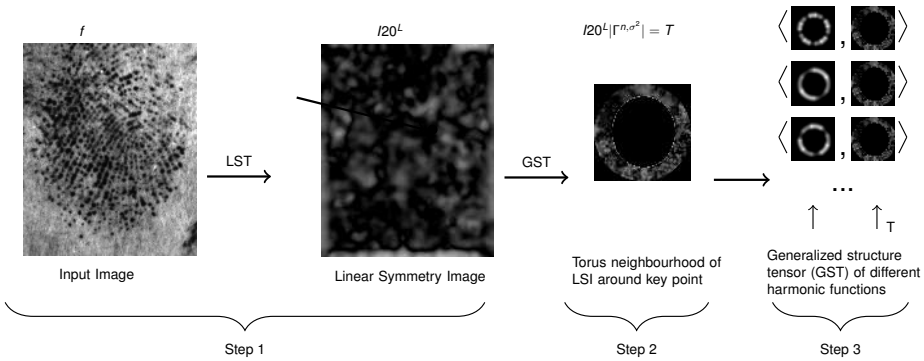

Figure 1: Steps of feature extraction for one torus.

orientation [BBN04], [Big88a] and is preferred to ST (real 2×2 matrix) because of its ability to generalize for extracting orientation in curvilinear coordinates easily. In this representation, LST becomes the simplest version of the Generalized Structure Tensor (GST) [BBN04] which is used in the steps that follow further below, detailed in Sections 2.2 - 2.3.

LST is a pair of scalars (at each pixel) embodying second-order (complex) moments of the local power spectrum in Cartesian coordinates

$$LST = (I_{20}^{(0)}, I_{11}^{(0)})^T = (\Gamma^{\{0,\sigma_{out}^2\}} * (\Gamma^{\{1,\sigma_{in}^2\}} * f)^2, |\Gamma^{\{0,\sigma_{out}^2\}}| * |\Gamma^{\{1,\sigma_{in}^2\}} * f|^2)^T \quad (1)$$

Here,

$$\Gamma^{\{n,\sigma^2\}} = (D_x + iD_y)^n e^{-\frac{r^2}{2\sigma^2}} = r^n \frac{1}{\kappa} e^{-\frac{r^2}{2\sigma^2}} e^{in\varphi} \quad (2)$$

is the n^{th} symmetry derivative[2] of a Gaussian, evaluating to an ordinary Gaussian function when $n = 0$. The function f is the image. The variance σ_{out}^2 fixates the size of the neighborhood in which the LST is extracted. The variance σ_{in}^2 fixates the inner scale or frequency characteristics of the nonlinear filter which ${I_{20}}^{(0)}$ constitutes with respect to the original image.

Here $\sigma_{L,out}^2$ and σ_{in}^2 are iteratively adjusted by first computing the LST for fixed values of them. This allows an initial dense (and simultaneous) estimation of frequency and orientation, yielding (dense) and adaptive Gabor filter constructions producing local phase responses, which in turn produce an enhanced original. The procedure is reapplied to the enhanced original until orientation, LST, and spatial frequency maps converge [pam14].

Because of being fully automatic, the resulting orientation map (Fig. 2) is still imperfect in some areas (usually where two orientations cross, such as a non-fingermark pattern in the background with the fingermark, for example). However, due to the slow variation of orientations in most of the fingermark region (hue in Fig. 2), corresponding to ridge flow, changes direction slowly, it is realistic to assume that a human expert will prefer to

[2]This is defined as the operator $(D_x + iD_y)^n$

verify the orientation map and correct erroneously estimated orientation regions rather than tracing the ridges in the original gray images to improve orientation maps. However, we used the computed orientation images as is, in other words, without manual interventions, to quantify their discriminative power in fully automatic orientation estimation scenarios when comparing to minutiae matching techniques (where minutiae are extracted manually for fingermarks).

In the LST of the preprocessing step, a Gaussian filter defines the outer scale. The spatial support can be seen as a small circular neighborhood as highlighted and marked by the arrow in Fig. 2, *Left* with radius of circle equal to $\sigma^2_{L,out}$. This radius is significantly smaller than the radii of rings on which the orientation will be modelled in the next section, $\sigma^2_{k,out}$, Fig. 2, *Right*.

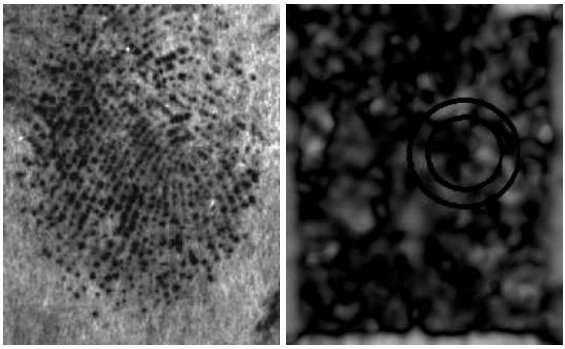

Figure 2: Original fingermark image and its corresponding linear symmetry image.

The processing results in one complex valued image, $I^{(0)}_{20}$, and one positive real image, $I^{(0)}_{11}$, representing the enhanced orientation densely. Complex pixel values of the $I^{(0)}_{20}$ image/matrix represent the orientation map depicting (twice) the direction of ridges in the fingermarks in pixel arguments, and the difference of costs between worst and best direction fit within the region determined by $\sigma^2_{L,out}$ where statistics of $I^{(0)}_{20}$ have been aggregated. Values of $I^{(0)}_{11}$ measure the strength of the image signal within the same region. We use the $I^{(0)}_{11}$ image to (pointwise) normalize complex values of $I^{(0)}_{20}$

$$I^L_{20} = \frac{I^{(0)}_{20}}{I^{(0)}_{11}}, \text{ where } |I^L_{20}| \leq 1 \tag{3}$$

It can be shown that the inequality holds with equality if and only if the orientation fit is error free [BBN04]. Fig. 2, *Right* shows I^L_{20} with hue/color representing orientation and value/intensity representing the quality of orientation map $|I^L_{20}|$.

2.2 Feature extraction as projection on harmonic functions and GST

Any complex analytic function g can be represented via two real harmonic functions ξ, η [Big88b]:

$$g(z) = \xi(x, y) + i\eta(x, y), \text{ where } z = x + iy. \tag{4}$$

Such harmonic function pairs ξ, η are locally orthogonal and their linear combinations, $a\xi + b\eta = const$, generate curve families with well-defined directions with respect to ξ, η, fixed by a, b. In particular, for any $1D$ function $s(t)$, one can generate "oriented" and symmetric curve families patterns, for example fixing s as a sine function and choosing g as $g(z) = \log(z)$ produces the family of spirals with different angles of twist, determined by a, b, representing orientation as shown in Fig. 3. Other examples of function $g(z)$ with s being a sinusoid are also shown.

Geometric transformations defined by harmonic pairs allow generalization of LST to detect symmetries beyond parallel line patterns. The generalization is a tensor representing curvilinear orientation, $\angle(a + ib)$, called a Generalized Structure Tensor (GST), and is defined as follows:

$$GST = (I_{20}^{(n)}, I_{11}^{(n)})^T = (\Gamma^{\{n,\sigma_{out}^2\}} * (\Gamma^{\{1,\sigma_{in}^2\}} * f)^2, |\Gamma^{\{n,\sigma_{out}^2\}}| * |\Gamma^{\{1,\sigma_{in}^2\}} * f|^2)^T, \tag{5}$$

where $\Gamma^{\{n,\sigma^2\}}$ is defined by (2). By changing n in the equation, in other words using different complex filters in the last convolution, it is possible to detect the presence of any harmonic curves, for example those in Fig. 3, and their respective orientation expressed as $2\angle(a+bi)$. The result is a pair of images, $(I_{20}^{(n)}, I_{11}^{(n)})$ representing the pattern (orientation and certainty of presence), wherein orientation is determined by $2\angle(a + bi)$.

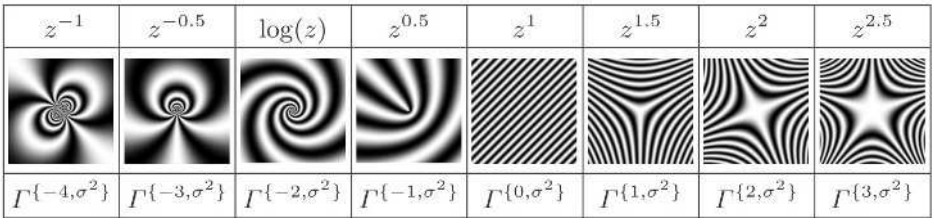

Figure 3: Set of harmonic functions with corresponding representation of structure tensor

Further, we choose the spatial supports of the filters, $|\Gamma^{n,\sigma^2}|$, radially and independent of the symmetry index, n, to model more regions around a key point in the hope to afford more unique identity for the point.

Accordingly, the local orientation image can be confined to a multiple tori. In a torus, the orientation content around an $h(x, y)$ key point can be expanded in a basis:

$$h(x, y) = \sum_k h_k(x, y), \text{ where } h_k(x, y) = \sum_n c_{kn}\psi_{kn}, \tag{6}$$

with

$$\psi_{kn} = r^{\mu_k} e^{-\frac{r^2}{2\sigma_k^2}} e^{-in\varphi}/\kappa_k \text{ and } c_{kn} =< \psi_{kn}, h_k > . \tag{7}$$

Here the image h_k is the confined orientation image defined as

$$h_k = |\psi_{kn}| \cdot I_{20}^L = |\psi_{kn}| \sum_n c_{kn} e^{-in\varphi}, \tag{8}$$

in which ψ_{kn} is identical to $\Gamma^{\{n,\sigma_k\}}$, except that $\|\psi_n\| = 1$ is assured via the normalization constant κ_k and that the constant n of the symmetry order is independent of the exponent, which is now represented by μ_k. The decoupling of n and μ_k is a necessity urged by the wish to define arbitrary tori, in which we want to describe the (image) orientation complexity at arbitrary symmetry level. Parameter $\sigma_{k,out}^2 = \sigma_k^2$ determines the radius of the k^{th} ring.

The advantage of this representation is that we can tune the outer scale filters used by GST to be of desired radius/size and width/compactness as in Fig. 2 *Right*, such that we can (mathematically) complete the description of orientation arbitrarily fine. In other words, we can change the peak radius, ring thickness, as well as the symmetry order μ_k as desired, to model the orientation information for different needs. The details on the relationship of μ_k, σ_k with radii and width of the filter are omitted due to space limitations.

The result of scalar products of harmonic filters ψ_{kn} with an orientation image neighborhood around a key point approximates the amount of presence of curve families, Fig. 3, in rings around the key point.

The feature vector is populated by using formula (7), where h_k is the normalized linear symmetry image I_{20}^L confined to a ring. The feature vector will be based on c_{kn}

$$c_{kn} =< \psi_{kn}, |\psi_{kn}| \cdot I_{20}^L >=< |\psi_{kn}|^2 e^{-in\varphi}, I_{20}^L >, \tag{9}$$

where σ_k^2 are determined by r_k, radius of $k-th$ torus and n.

Likewise, an additional set of coefficients e_k corresponding to energy in rings (I_{11}^L of Eq. (5)) can be obtained:

$$e_k =< |\psi_{kn}|^2, |h_k| > . \tag{10}$$

It is straight forward to show that e_k is constant when n changes. Hence it needs to be calculated only once per ring.

The extracted c_{kn} is normalized by e_k, resulting in a complex feature array $\mathbf{SAFE}$ with elements:

$$SAFE_{kn} = \frac{c_{kn}}{e_k} \in \mathbb{C}, \tag{11}$$

which is the suggested feature. By construction, $|SAFE_{kn}| \leq 1$ holds with equality if and only if a member of a single curve family (the one determined by n) describes h_k without error.

The dimension of the feature vector describing a key point is fixed by the number of rings and the size of projection base N_h inside each torus; in our case it equals to $N_f \times N_h$, since N_h is chosen to be the same for each torus.

With r_{min}, r_{max} being the smallest and largest radii, we sampled other radii equidistantly in exponential scale between $[r_{min}, r_{max}]$ to determine all tori peak positions once m is fixed as detailed next.

The fact that filter values are normalized via κ_k, such that $\|\psi_{kn}\| = 1$ makes feature vectors from the larger rings to have the same importance as those from smaller rings (see Fig. 4 for filter shapes and positions in the current application).

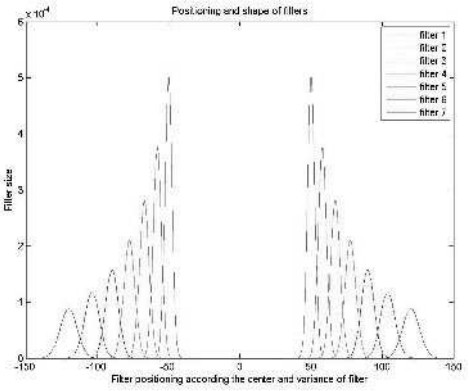

Figure 4: *Left:* Sample set of filters used for feature extraction in cores. Position of peaks, width of filters, and area of intersection are fixed.

2.3 Rotation invariance of the features

An important property of the suggested features is their rotation invariance in the sense that the features of a rotated image can be deduced from the features of the unrotated image if the rotation angle is known. A feature can then be made rotation invariant if the associated key point has an intrinsic orientation by aligning feature vector components to the intrinsic orientation. In our case, the core angle has been used as intrinsic orientation because we will extract a $SAFE$ for cores to illustrate its potential usefulness for recognition at the level of core identities. Since Equations (6) and (9) constitute a Fourier basis reconstruction of the torus orientation $\tilde{f}_k$, our features can be shown to be rotation invariant as follows:

$$SAFE'_{kn} = e^{2i(n+2)\varphi'} SAFE_{kn}, \tag{12}$$

where $\varphi' = \angle SAFE_{k,-1}$ represents the automatically computed parabolic symmetry orientation, modeling the estimated core orientation. The $SAFE'_{kn}$ features will then be rotation invariant allowing the rotation compensation procedure to be implemented by a simple multiplication at low cost (without image rotation).

Note that for n=-2 symmetry, log-spirals, there is no rotation compensation, which is also not necessary since the angles of these are (absolutely) rotation invariant by themselves.

3 Quality descriptors: data sufficiency and good model fit

The Structure Tensor operates in the complex space. Therefore, at every step we obtain complex valued results such as I_{20}^L in preprocessing stage, and $SAFE_{kn}$ in feature extraction step. The $SAFE_{kn}$ features differ from the commonly obtained real-valued feature vectors since the complex number magnitudes always represent quality measurements.

As was described in Sec. 2.1, the structure tensor at an image point comprises the orientation vector $I_{20}^{(0)}$ and the signal strength $I_{11}^{(0)}$. The complex scalar $I_{20}^{(0)}$ represents the directional dominance within its outer scale or the direction of major eigenvector, which follows from the following eigenvalue, eigenvector direction representation of LST, [Big87]:

$$\begin{aligned} I_{20}^{(0)} &= (\lambda_{max} - \lambda_{min}) e^{2i\varphi_{max}} \\ I_{11}^{(0)} &= \lambda_{max} + \lambda_{min}. \end{aligned} \tag{13}$$

Let us consider the case $\lambda_{min} = 0$ and $\lambda_{max} \gg 0$, which stems from a local image with well-defined direction of isocurves being perfectly parallel. From Eq. (13) it follows that $|I_{20}^{(0)}| = I_{11}^{(0)}$ for the ideal case of perfect linear symmetry (see Fig. 3). Accordingly, the vectorial summation magnitude $|I_{20}^{(0)}|$ would be strictly less than $I_{11}^{(0)}$ if the isocurves would not be perfectly parallel. Thereby, normalization of the complex valued $I_{20}^{(0)}$ by $I_{11}^{(0)}$ yields a local quality measure, the statistics of which have been used to estimate the global quality of a fingerprint [TW05], [FKB06].

In other words, $|I_{20}^L|$ automatically demonstrates the amount of agreement between the model and the (noisy) data. It is also bounded to be within a $[0, 1]$ interval.

Further, by using $\tilde{f}_k = I_{20}^L \cdot |\psi_{kn}|$, which is independent of n and is the orientation map multiplied with torus, we make sure that image information inside N_f rings is "marked" for lack of data. This is needed to properly summarize the quality inside every ring so that quality measures from different rings share the same "quality scale". Therefore, if an extraction ring will miss some part of an image (for example, if a key point is close to the boundary of the image, the ring will cover non-image areas), the quality metric will reflect that in $I_{11}^{(0)}$. For instance, since the image is set to zero outside of its boundaries, the feature vector components will be less than 1, in their magnitudes. This is because it can be shown that all harmonic wave families fulfill (via Schwarz inequality) the following:

$$|c_{kn}| = |\langle \psi_{kn}, \tilde{f}_k \rangle| = |\langle \psi_{kn}, |\psi_{kn}| \cdot I_{20}^L \rangle| \leq \langle |\psi_{kn}|, |\psi_{kn}| \cdot |I_{20}^L| \rangle = e_k \leq 1. \tag{14}$$

The first inequality is because $I_{20}^L \leq 1$, Eq. (3) and $\|\psi_{kn}\| = 1$. Hence both $|c_{kn}|$, e_k, and c_{kn}/e_k, are bounded by 1. If and only if there is sufficient data ($|I_{20}^L|$) in the entire ring, will e_k reach the value 1, and only if the model fits perfectly well will $|c_{kn}|$ reach e_k. Thus $|SAFE_{kn}|$ measures both data sufficiency and the goodness of model fit.

4 Matching

For every key point, we have introduced an $N_f \times N_h$ complex feature vector. Our matching score comprising the distance between reference ($r \in \mathbb{C}$) and test ($t \in \mathbb{C}$) features is based (again) on the tight inequality between the scalar products:

$$MS = \frac{< \boldsymbol{SAFE}^r, \boldsymbol{SAFE}^t >}{< |\boldsymbol{SAFE}^r|, |\boldsymbol{SAFE}^t| >} \in \mathbb{C}. \tag{15}$$

For the introduced matching metric, we obtain the complex matching score $MS = a + bi$, where $\angle(a + bi)$ measures the angle between two arrays with $N_f \times N_h$ complex elements each, and $|a + bi|$ shows the confidence in the measured global angle.

However, for a true pair of feature arrays, the matching score should yield a real and positive number 1, in other words $\angle(a + bi) = 0$. Generally, the argument angles are within $[0, 2\pi]$, and the confidence measure is in an $[0, 1]$ interval.

To fuse both confidence and the angle into a matching score, we therefore take the real part of MS:

$$\hat{MS} = Re(MS) = |MS| cos(\angle MS) \in [-1, 1], \tag{16}$$

where $MS = -1$ means maximal mismatch and $MS = 1$ means perfect match.

5 Experiments

5.1 Database

For testing SAFE descriptors, we have employed the only publicly available forensic fingerprint database, that of the NIST SD27 [Gar]. It includes 258 pairs of (mated) fingermark and fingerprint images. We selected images having either cores or loops (two cores) with a total 263 core pairs in 201 mated fingerprint pairs. Cores (as well as minutiae) have well-defined directions, while for other fingerprint patterns the intrinsic angle may not exist (e.g., perfect whorls) or not be unique (e.g., perfect deltas). The suggested feature vector can model key points having strong orientation variation in its surrounding area.

The more complex the orientation variation the more unique identity can be given by the feature vector to the key point. This has motivated the use of core points as our test bed. Additionally, core points allow examination of rotation invariance of the features conveniently. However, even neighborhoods of minutiae and other key points can be described by SAFE features, if some strong intrinsic orientation exists in any ring.

5.2 Performance

We have sampled the $[2, 97]$ interval into 9 exponentially growing radii representing peaks of tori and selected empirically the largest three tori; in other words, we chose $N_f = 3$ with radii $r = [27, 41, 63]$, respectively reflecting the fact that the fingermarks have bad quality in rings close to core points. For the SD27 fingermark database, our feature vector is a 3×9 array. More than 3 radii can be set fixed in tenprints and the expert can include/exclude the rings of a fingermark in a real scenario to match the newly constructed feature vector of a key point in the fingermark with pre-calculated features of the tenprint database. However, we have refrained from this (manual interference) in our experiments.

We performed client and impostor tests on 262 core points (corresponding to $33,092$ impostor verification tests) and observed an EER of 24%, Fig. 5, *Left*. It is worth noting that verification is at core level, and due to the low quality of the fingermarks and the high number of impostor tests, SAFE descriptors must equip each core with sufficiently unique identity power. Thus, equal error rate demonstrates the amount of erroneously recognized cores in the presence of massive core impostors. This is a good performance level with *only* orientation image information around single key point because more key points and minutiae can be used to recognized a fingermark.

It is problematic to relate the present features to other methods because the few published studies use incomparably more manual interference (manually extracted minutiae) or sufficiently more key points (minutiae constellations), but less image information in combination with matching software that are either proprietary or closed. The observed EER using a publicly available (source code) minutiae-only matcher shows 36% EER [MB12] performance on an ideal set (and 6% on a matched set - which is an unrealistic scenario), which is significantly poorer than the achievement of the suggested method. The number of images that is used differs in comparison with the protocol, but the goal of the paper is to present the new concept of feature extraction. Further experiments on multiple minutiae are required for benchmarking present work.

At the same time, forensic applications use rank-k identification rate, Fig. 5, *Right*. In [PFJ13], a (manually matched) minutiae constellation together with extended minutiae-based information are used to achieve rank-20 67% identification of *fingermark*, while we are (currently) using a single point, but more image information to identify *cores*, resulting in rank-20 58%. Most interestingly, our study concerns novel *image-based* features which can be complementary to minutiae information.

Power of the feature is the ability to provide additional automatically extracted information on images of poor quality; therefore, experiments are performed on forensic fingerprints only, with ground truth information known.

In this paper we provide experiments for a core of the image to demonstrate the power of a single point with increased orientation information. Suggested feature extracted around the core can serve as a source of additional information for low quality noisy images if a core was detected. Future work will include experiments on extending traditional features of minutiae with the SAFE feature.

The feature predictably failed for the images where the automatic orientation map failed,

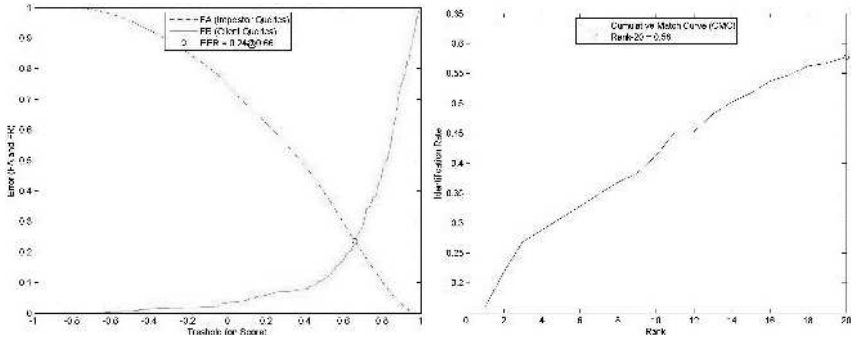

Figure 5: EER and CMC curves of matching core points for the SD27 database

in other words, for smudged images, or images with an intersecting background of similar frequency.

6 Conclusions and future work

We have proposed a novel feature extraction method that shows good discrimination ability of key points on bad quality images (of SD27 forensic fingerprint database). The SAFE descriptors go beyond matching point locations and orientations alone, and utilize characteristics of the image's surrounding points. The proposed features have built-in quality estimates as well as rotation invariance.

Results of matching forensic fingerprints indicate that similar features can be constructed for other applications, such as for small contact area fingerprint sensors, irises, faces and shoeprints, for example.

The current version of the algorithm can automatically extract image information without manual intervention. Future work will include increasing the amount of key points to more than one in order to improve the performance; as well as experiments on extending features of minutiae, angle, and position, with the suggested feature. We also plan to investigate the effect of the feature when applying it to other types of images, such as irises, for example.

References

[BBN04] Josef Bigun, Tomas Bigun, and Kenneth Nilsson. Recognition by symmetry derivatives and the generalized structure tensor. *Pattern Analysis and Machine Intelligence, IEEE Transactions on*, 26(12):1590–1605, 2004.

[Big87] Josef Bigun. Optimal orientation detection of linear symmetry. 1987.

[Big88a] Josef Bigun. Pattern recognition by detection of local symmetries. *Pattern Recognition and Artificial Intelligence*, pages 75–90, 1988.

[Big88b] Josef Bigun. Recognition of local symmetries in gray value images by harmonic functions. In *Pattern Recognition, 1988., 9th International Conference on*, pages 345–347. IEEE, 1988.

[BVG+00] Asker M Bazen, Gerben TB Verwaaijen, Sabih H Gerez, Leo PJ Veelenturf, and Berend Jan van der Zwaag. A correlation-based fingerprint verification system. 2000.

[CCG05] Sharat Chikkerur, Alexander N Cartwright, and Venu Govindaraju. K-plet and coupled BFS: a graph based fingerprint representation and matching algorithm. In *Advances in Biometrics*, pages 309–315. Springer, 2005.

[CCHW97] Shih-Hsu Chang, Fang-Hsuan Cheng, Wen-Hsing Hsu, and Guo-Zua Wu. Fast algorithm for point pattern matching: invariant to translations, rotations and scale changes. *Pattern recognition*, 30(2):311–320, 1997.

[CFM10] Raffaele Cappelli, Matteo Ferrara, and Davide Maltoni. Minutia cylinder-code: A new representation and matching technique for fingerprint recognition. *Pattern Analysis and Machine Intelligence, IEEE Transactions on*, 32(12):2128–2141, 2010.

[FAMSAFOG05] Julian Fierrez-Aguilar, LM Munoz-Serrano, Fernando Alonso-Fernandez, and J Ortega-Garcia. On the effects of image quality degradation on minutiae-and ridge-based automatic fingerprint recognition. In *Security Technology, 2005. CCST'05. 39th Annual 2005 International Carnahan Conference on*, pages 79–82. IEEE, 2005.

[FKB06] Hartwig Fronthaler, Klaus Kollreider, and Joseph Bigun. Automatic image quality assessment with application in biometrics. In *Computer Vision and Pattern Recognition Workshop, 2006. CVPRW'06. Conference on*, pages 30–30. IEEE, 2006.

[Gar] Michael D Garris. Latent Fingerprint Training with NIST Special Database 27 and Universal Latent Workstation NISTIR 6799.

[JY00] Xudong Jiang and Wei-Yun Yau. Fingerprint minutiae matching based on the local and global structures. In *Pattern Recognition, 2000. Proceedings. 15th International Conference on*, volume 2, pages 1038–1041. IEEE, 2000.

[MB12] Anna Mikaelyan and Josef Bigun. Ground truth and evaluation for latent fingerprint matching. In *Computer Vision and Pattern Recognition Workshops (CVPRW), 2012 IEEE Computer Society Conference on*, pages 83–88. IEEE, 2012.

[pam14] Dense frequency maps by structure tensor and logarithmic scale space: application to forensic fingerprints. *submitted to Transactions on Pattern Analysis and Machine Intelligence*, 2014.

[PFJ13] Alessandra A Paulino, Jianjiang Feng, and Anil K Jain. Latent fingerprint matching using descriptor-based hough transform. *Information Forensics and Security, IEEE Transactions on*, 8(1):31–45, 2013.

[RBPV00] Nalini K Ratha, Ruud M Bolle, Vinayaka D Pandit, and Vaibhav Vaish. Robust fingerprint authentication using local structural similarity. In *Applications of Computer Vision, 2000, Fifth IEEE Workshop on.*, pages 29–34. IEEE, 2000.

[TW05] Elham Tabassi and Charles L Wilson. A novel approach to fingerprint image quality. In *Image Processing, 2005. ICIP 2005. IEEE International Conference on*, volume 2, pages II–37. IEEE, 2005.